frontiers | Frontiers in Marine Science

TYPE Original Research
PUBLISHED 13 January 2023
DOI 10.3389/fmars.2022.1101599



OPEN ACCESS

EDITED BY
Dong Feng,
Shanghai Ocean University, China

REVIEWED BY
Yao Guan,
Ministry of Natural Resources, China
Jiasheng Wang,
China University of Geosciences Wuhan, China

*CORRESPONDENCE
Xiaoming Sun
eessxm@mail.sysu.edu.cn
Li Xu
xuli22@mail.sysu.edu.cn

†These authors share first authorship

SPECIALTY SECTION
This article was submitted to Marine Biogeochemistry, a section of the journal Frontiers in Marine Science

RECEIVED 18 November 2022
ACCEPTED 15 December 2022
PUBLISHED 13 January 2023

CITATION
Yang X, Zhang Y, Sun X, Xu L and Chen T (2023) Marine sediment nitrogen isotopes and their implications for the nitrogen cycle in the sulfate-methane transition zone. *Front. Mar. Sci.* 9:1101599. doi: 10.3389/fmars.2022.1101599



# Marine sediment nitrogen isotopes and their implications for the nitrogen cycle in the sulfate-methane transition zone

Xin Yang[1,2], Yihao Zhang[2,3†], Xiaoming Sun[1,2,3*], Li Xu[1,2*] and TingTing Chen[1,2]

[1]School of Marine Sciences, Sun Yat-sen University, Zhuhai, China, [2]Guangdong Provincial Key Laboratory of Marine Resources and Coastal Engineering, Zhuhai, China, [3]School of Earth Science and Engineering, Sun Yat-sen University, Zhuhai, China

**Introduction:** Recent work has proposed that the nitrogen isotopes in marine sediments can be impacted by anaerobic oxidation of methane (AOM), since nitrogen uptake by anaerobic methanotrophic archaea (ANME) modifies the nitrogen isotope compositions of bulk sediment. Thus, unraveling the AOM-driven nitrogen cycle in the sulfate-methane transition zone (SMTZ) becomes significant. Additional study of the nitrogen cycle between sediment and interstitial water in SMTZ is needed.

**Methods:** To better understand the nitrogen cycle in the SMTZ, we analyzed NH4+ concentrations of interstitial water and nitrogen isotopes of sediment in the core GC10 from the southwestern Taiwan Basin in the South China Sea.

**Results:** The defined SMTZ is located at 560–830 cmbsf, based on methane and sulfate concentrations, as well as TS/TOC ratios, δ13CTIC and δ34S values. In the SMTZ, the NH4+ concentration decreases, the δ15NTN shows a negative excursion, δ15Ndecarb displays a positive excursion.

**Discussions:** NH4+ concentration decrease is interpreted by sulfate-reducing ammonium oxidation (SRAO). The δ15NTN shows negative excursion, which is most likely interpreted to N2 (δ15N=0‰) released from SRAO that was fixed into marine sediment via ANME nitrogen fixation. The δ15Ndecarb shows a negative correlation with NH4+ concentrations, indicating that it was controlled by organic matter decomposition. In the SMTZ, the methane competes with organic matter for becoming the substrate of sulfate reduction bacteria, which possibly decreases the organic matter degradation rate and causes δ15Ndecarb relative positive excursion. Although δ15Ndecarb is controlled by organic matter degradation, δ15NTN still reveals a negative excursion in the SMTZ. This likely indicates that nitrogen uptake by ANME/AOM microbial consortiums mainly modifies the nitrogen isotope of soluble nitrogen in the SMTZ.

**Conclusions:** This study indicates unique geochemistry processes in SMTZ will modify nitrogen characteristics in sediment/interstitial water, and the latter can serve as a proxy for AOM.

KEYWORDS

cold seep, anaerobic oxidation of methane (AOM), nitrogen isotopes, total organic carbon (TOC), South China Sea

## 1 Introduction

Methane ($CH_4$) is a strong greenhouse gas, with 25 times more greenhouse effects than carbon dioxide over 100 years (IPCC, 2007; Ruppel, 2017). Methane is the main component of gas hydrate deposits (Ruppel, 2017). Gas hydrates tend to form in a low-temperature and high-pressure environment with sufficient methane concentrations (Clennell et al., 1999). The continental margin is highly conducive to gas hydrate formation and represents the world's largest gas hydrate reservoirs (Suess, 2010). The buried gas hydrate is unstable, and would decompose due to various processes, such as earthquakes and ocean current circulation (Suess, 2020). Gas hydrate decomposition would generate a methane flow transported from deeper sediments towards the seafloor, which is called methane leakage (Suess, 2020). Methane leakage adds about 0.02 Gt of carbon to the ocean each year (Boetius and Wenzhöfer, 2013). Methane leakage is widely dispersed across the continental margin and has had a major impact on marine carbon cycling and climate over the last geological history (Dickens, 2003; Levin et al., 2016; Ruppel, 2017; Egger et al., 2018; Zhang et al., 2019; Akam et al., 2020; Kim and Zhang, 2022). Most of the methane released is consumed by anaerobic oxidation of methane (AOM) in the shallow sediments and/or anoxic water column, primarily using sulfate as an electron acceptor (Boetius et al., 2000; Reeburgh, 2007). The AOM process will occur at the sulfate methane transition zone (SMTZ), mediated by sulfate reducing bacteria (SRB) and anaerobic methanotrophic archaea (ANME) (Boetius et al., 2000). During this process, authigenic pyrite and carbonate are generated, significantly changing the sediment's geochemical characteristics (Boetius et al., 2000; Peckmann and Thiel, 2004; Lin et al., 2016). At the SMTZ, multiple elements (C, O, N, P, Fe, Mo etc.) undergo unique geochemical turnover (Peckmann et al., 1999; Boetius et al., 2000; Antler et al., 2015; Feng et al., 2018a; Feng et al., 2018b), understanding which is of great significance to tracing methane leakage.

Nitrogen is a fundamental element for life (Jing et al., 2020). Nitrogen is contained in all life (Jing et al., 2020). In the SMTZ, nitrogen experiences complex biogeochemical interactions, and the nitrogen isotope composition of sediments can be modified by ANME or AOM microbial consortiums (Dekas et al., 2009; Ettwig et al., 2010; Dong et al., 2017; Hu et al., 2020). Laboratory culture results have revealed that ANME can mediate nitrogen fixation and ammonia assimilation (Dekas et al., 2009). Recent studies suggest that nitrogen uptake by ANME causes a negative excursion of nitrogen stable isotopes in sediment (Feng et al., 2015; Hu et al., 2020), which can be applied as a proxy for AOM-impacted sediment in settings with or without authigenic carbonates (Hu et al., 2020). Previous studies mainly focused on nitrogen isotopic compositions in sediments or cold-seep organisms (Feng et al., 2015; Hu et al., 2020), whereas similar studies on sediment-interstitial water are rare.

Although ANME could mediate nitrogen fixation and lead to a negative excursion of biomass $\delta^{15}N$, the $\delta^{15}N$ composition in marine sediments could also be affected by both sedimentary input and diagenesis processes (Wehrmann et al., 2011; Robinson et al., 2012; Quan et al., 2013a; Quan et al., 2013b). The $\delta^{15}N$ compositions of marine sediments can be influenced by different nitrogen inputs (Quan et al., 2013b; Quan et al., 2013a; Tesdal et al., 2013). Redox conditions could also influence the $\delta^{15}N$ compositions of marine sediments (Quan et al., 2013b). Nitrate utilization and denitrification can also result in large nitrogen isotope fractionation (up to 30‰) (Freudenthal et al., 2001; Lehmann et al., 2002; Lehmann et al., 2007; Robinson et al., 2012). The diagenesis process would also have an impact on $\delta^{15}N$ of marine sediment (Freudenthal et al., 2001; Lehmann et al., 2002; Robinson et al., 2012). Organic matter degradation includes preferential degradation of amino acids rich in $^{15}N$ (Nakatsuka et al., 1997) and selective removal of proteins (Macko and Estep, 1984), which could induce $\delta^{15}N$ of organic matter decrease. Therefore, the nitrogen cycle between sediment and interstitial water may be more complicated than previously thought. It is necessary to combine interstitial water data and sediment data to uncover the nitrogen cycle in SMTZ.

In this study, we analyzed the nitrogen concentrations, nitrogen isotopic compositions of marine sediment as well as the $NH_4^+$ concentration in interstitial water. The object of this study is to understand the mechanism of the nitrogen cycle in SMTZ.

## 2 Geological setting

The sampling site (core GC10) is located in the southwestern Taiwan basin of the northeastern South China Sea (Figure 1).

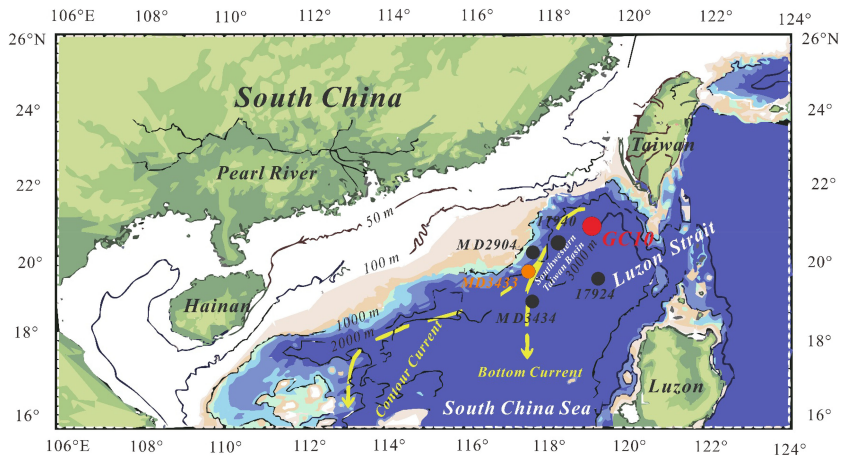


FIGURE 1
Map showing the sampling locations (red spot) *(modified after* Xu et al., 2021).

The basin has a 7 km-thick sediment succession with abundant organic matter and a high geothermal gradient, favoring gas hydrate formation (McDonnell et al., 2000). Moreover, bottom simulating reflectors (BSR) are widely distributed in the basin, indicating buried gas hydrates (McDonnell et al., 2000; Wu et al., 2007). The Jiulong methane reef was discovered in the southwestern Taiwan basin, and gas hydrates were successfully drilled in 2013 (Tong et al., 2013; Lin et al., 2018b). The Jiulong reef represents the world's largest methane-derived authigenic carbonate reef, indicating methane seepage used to be a common process at this site (Zhang et al., 2015). The southwestern Taiwan basin is considered a highly promising gas hydrate exploration target in the South China Sea (Lin et al., 2021).

## 3 Material and methods

The piston core was collected at site GC10 (21°18.453'N, 119°11.819'E) in the southwestern Taiwan basin in the South China Sea during the "Taiyang" cruise (No. SO177, June, 2004). The water depth at GC10 is 3008 m, and the core is 9.37 m long. The "porridge structure" is present at 9.10–9.20 m depth, likely caused by gas hydrate dissociation (Wu et al., 2010). The sediments are composed mainly of silt and fine-grained clay. After the retrieval, the core was cut into ~10 cm intervals and stored in a cold room (4°C). Samples were packed individually in zip-lock plastic bags and freeze-dried. For elemental and isotopic analyses, the samples were selected at 30 cm intervals, and pulverized with an agate mortar to< 63 μm.

Total sulfur (TS) and total nitrogen (TN) content were measured with a CNS-HO rapid element analyzer at the Guangdong Provincial Key Laboratory of Marine Resources and Coastal Engineering in March 2021. About 30 mg of the sample (mixed with ~30 mg $V_2O_5$) was transferred to a tin cup (2 mm*8 mm), and then converted to $SO_2$ and $N_2$ at 1020°C before being measured by the element analyzer.

Total organic carbon (TOC) and decarbonated nitrogen ($N_{decarb}$) contents were measured by an elemental analyzer. About 0.2 g of sediment was added into a 15 mL centrifuge tube and acidified by about 15 mL of 10% HCl (excess) for 12 hours, and then washed three times with deionized water. The treated samples were freeze-dried for TOC and $N_{decarb}$ content measurement, with analytical procedures similar to those for the TS and TN measurements.

The TS, TN, TOC, and $N_{decarb}$ isotopes were determined with a continuous flow Thermo Fisher Scientific MAT 253 Plus isotope ratio mass spectrometer at the School of Marine Sciences, Sun Yat-Sen University, in March 2021. About 15 mg of the sample was converted to $CO_2$, $SO_2$, $N_2$ in the elemental analyzer at 1020°C, and then the isotope compositions were measured by the isotope ratio mass spectrometer. $N_{other}$ content was calculated by subtracting $N_{decarb}$ from TN content. $N_{other}$ isotope values were calculated by the simple binary model:

$$\delta_{TN} * £_{TN} = \delta_{decarb} * £_{decarb} + \delta_{other} * £_{other}$$

Where δ represents the nitrogen isotope value; £ represents the nitrogen content.

Total inorganic carbon (TIC) isotopes were measured by a Thermo Fisher Scientific MAT 253 Plus isotope ratio mass spectrometer coupled with the Gas Bench II. Bulk sediment (~800 μg) was placed into a clear glass centrifuge tube, and helium gas was applied to flush out atmospheric gases from the tube. About 5 mL of 100% phosphoric acid was added to the tube at room temperature (25°C). In the tube, carbonate in sediments reacted with phosphoric acid for 24 hours, and then the released $CO_2$ was transported *via* Gas Bench II to be analyzed by the mass spectrometer.

The C, S, and N isotope values were reported with the standard δ notation relative to the Vienna Pee Dee Belemnite (V-PDB), Vienna Canyon Diablo Troilite (V-CDT), and atmospheric nitrogen, respectively. International reference materials for the C, S, and N isotopic data calibration are IAEA-S1 ($\delta^{34}S$ = −0.30‰), NBS-18 ($\delta^{13}C$ = −5.014‰, $\delta^{18}O$ = −23.2‰) and IAEA-600 ($\delta^{13}C$ = -27.771‰, $\delta^{15}N$ = 1.0‰), respectively.

We compiled $NH_4^+$, methane, and sulfate concentrations from Wu et al. (2010) to reflect the nitrogen cycle and biochemical rate (Wu et al., 2010). Porewater was squeezed from marine sediment after retrieval (Wu et al., 2010). The $NH_4^+$ concentration of porewater was measured by a spectrophotometer on deck in June 2004 (Wu et al., 2010). Methane and sulfate concentrations were measured by ICP at the Guangzhou Marine Geological Survey in July 2004 (Wu et al., 2010). The precision of porewater is available for numerical simulation and analysis.

In this study, the organic matter degradation rate ($R_{POC}$), OSR rate, AOM rate, and methanogenesis rate under steady-state were calculated using porewater data and TOC content (Table S1–S4; Figure 2). The geochemistry rate models used in this study were the most well-known and commonly used in AOM-impacted sediment cores (Lehmann et al., 2002; Wehrmann et al., 2011; Meister et al., 2019; Zhang et al., 2019; Akam et al., 2020; Zhang et al., 2021). The parameters used in those models are as close to the study site as possible.

The organic matter degradation rate, $R_{POC}$ (g C $g^{-1}$ $yr^{-1}$), was calculated based on the most accepted method (Middelburg, 1989; Borowski et al., 1996; Beulig et al., 2017).

$$R_{POC} = POC * \left(0.16 * \left(a_0 + \frac{x}{v_s}\right)^{-0.95}\right) \quad (1)$$

Where $a_0$ is the initial age of organic matter ($a_0$ = 6030 yr BP; Table S1); $x$ (cm) represents the depth below seafloor; $v_s$ is the porewater downward diffusion velocity, in this study, $v_s$ equal to sedimentary rate (cm $yr^{-1}$) ($v_s$=25 cm $yr^{-1}$); POC is the TOC content of sediment.

The rate of AOM (Boetius et al., 2000), $R_{AOM}$ (μmol $cm^{-3}$ $yr^{-1}$), was calculated based on the most accepted method (Regnier et al., 2011):

$$R_{AOM} = k_{AOM} * \left[SO_4^{2-}\right] * [CH_4] \quad (2)$$

Where $K_{AOM}$ is the rate constant ($k_{AOM}$=1, according to Luo et al., 2015); $[SO_4^{2-}]$ and $[CH_4]$ are the concentrations of sulfate and methane in porewater (Table S2).

Based on the previous studies (Middelburg, 1989; Beulig et al., 2017), the rate of methanogenesis was determined as follows:

$$R_{MG} = 0.5 * \frac{\rho_s * (1 - \varnothing) * 10^6}{MW_C * \varnothing} * \frac{\left[SO_4^{2-}\right]}{\left[SO_4^{2-}\right] + K_{SO_4^{2-}}} * R_{POC} \quad (3)$$

Where $\rho_s$ is the density of dry sediment ($\rho_s$ =2.5 g/$cm^3$; according to Luo et al., 2015); ∅ is the porosity of sediment (∅ =0.7; according to Feng et al., 2021); $MW_C$ is the atomic weight of carbon (12 g/mol); $K_{SO_4^{2-}}$ is the Michaelis–Menten constant ($K_{SO_4^{2-}}$ = 0.1).

Age data were compiled to constrain the initial age of organic matter and the sedimentary rate (Table S1). The parameters of models are listed in Table S2 (Table S2).

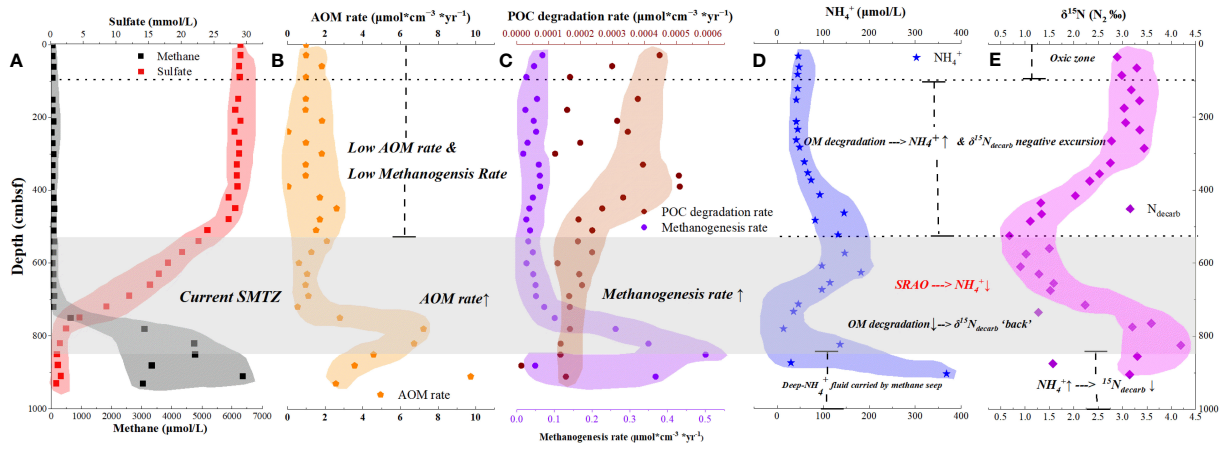


FIGURE 2
Graph for geochemistry rates, NH4+ concentration, and Ndecarb isotope composition. **(A)** Methane and sulfate concentrations in GC10. **(B)** AOM rate of GC10. AOM rate increases in the SMTZ. **(C)** Organic matter degradation rate and methanogenesis rate of GC10. The organic matter degradation rate decreases with depth due to the organic matter's decreased reactivity. The methanogenesis rate increases sharply in the SMTZ. **(D)** NH4+ concentrations of GC10 (Wu et al., 2010). In 0–560 cmbsf, NH4+ concentration increases with depth; in 560-830 cmbsf, NH4+ concentration display a distinct drop; below 830 cmbsf, NH4+ concentration sharply increases. **(E)** δ15Ndecarb shows a negative correlation with NH4+ concentration.

# 4 Results

## 4.1 Carbon and sulfur isotope compositions

The $\delta^{13}C_{TIC}$ of sediment from site GC10 is presented in Figure 3D. The $\delta^{13}C_{TIC}$ values vary widely, ranging from -20.89 to 1.03‰, averaging -2.37‰ (n = 32). In 0-420 cmbsf, the $\delta^{13}C_{TIC}$ is relatively stable, averaging 0.19‰ (n = 14). In 440-560 cmbsf, the $\delta^{13}C_{TIC}$ also shows relatively stable values, averaging -3.24‰ (n = 5). Distinct negative $\delta^{13}C_{TIC}$ excursions occur at 630 and 730 cmbsf, which reach -20.33‰ and -20.89‰, respectively. Below 830 cmbsf, the $\delta^{13}C_{TIC}$ of sediment displays relative stability, averaging -0.6‰ (n = 3). The $\delta^{34}S$ of sediment from site GC10 is presented in Figure 3E. Bulk sediment $\delta^{34}S$ varies from -29.36 to 24.20‰, averaging 4.20‰ (n = 32). The $\delta^{34}S$ is stable in 0–100 cmbsf (from 9.27 to 9.69‰; avg. 9.46‰; n = 3), decreases with depth in 100–400 cmbsf (from 9.46 to -27.96‰), and increases with depth in 400–930 cmbsf (from -27.96 to 24.2‰) (Figures 3D, E; Tables 1, 2).

TABLE 1 C-N-S content of core GC10.

| Depth (cmbsf) | TOC content (wt%) | TN content (wt%) | Ndecarb content (wt%) | Nother content (wt%) |
|---|---|---|---|---|
| 30-40 | 0.54 | 0.15 | 0.08 | 0.07 |
| 60-70 | 0.53 | 0.12 | 0.08 | 0.04 |
| 80-90 | 0.39 | 0.13 | 0.06 | 0.07 |
| 117-130 | 0.4 | 0.11 | 0.06 | 0.05 |
| 150-160 | 0.5 | 0.14 | 0.08 | 0.06 |
| 167-177 | 0.43 | 0.1 | 0.03 | 0.07 |
| 208-220 | 0.5 | 0.14 | 0.08 | 0.06 |
| 230-242 | 0.6 | 0.13 | 0.08 | 0.05 |
| 260-270 | 0.37 | 0.13 | 0.05 | 0.08 |
| 280-290 | 0.24 | 0.12 | 0.03 | 0.09 |
| 320-330 | 0.84 | 0.19 | 0.11 | 0.08 |
| 350-360 | 0.87 | 0.17 | 0.11 | 0.06 |
| 370-380 | 0.92 | 0.19 | 0.11 | 0.08 |
| 410-420 | 0.63 | 0.15 | 0.08 | 0.07 |
| 429-440 | 0.53 | 0.14 | 0.08 | 0.06 |
| 460-470 | 0.4 | 0.15 | 0.06 | 0.09 |
| 479-490 | 0.51 | 0.13 | 0.08 | 0.05 |
| 520-530 | 0.43 | 0.2 | 0.07 | 0.13 |
| 550-560 | 0.43 | 0.13 | 0.07 | 0.06 |
| 570-580 | 0.49 | 0.13 | 0.08 | 0.05 |
| 605-615 | 0.31 | 0.11 | 0.05 | 0.06 |
| 625-632 | 0.55 | 0.06 | 0.09 | – |
| 652-660 | 0.53 | 0.12 | 0.07 | 0.05 |
| 670-680 | 0.44 | 0.14 | 0.06 | 0.08 |
| 710-720 | 0.46 | 0.11 | 0.06 | 0.05 |
| 730-740 | 0.22 | 0.08 | 0.03 | 0.05 |
| 760-770 | 0.34 | 0.1 | 0.04 | 0.06 |
| 775-790 | 0.49 | 0.15 | 0.06 | 0.09 |
| 820-830 | 0.42 | 0.12 | 0.06 | 0.06 |

*(Continued)*

TABLE 1 Continued

| Depth (cmbsf) | TOC content (wt%) | TN content (wt%) | Ndecarb content (wt%) | Nother content (wt%) |
|---|---|---|---|---|
| 850-860 | 0.43 | 0.12 | 0.05 | 0.07 |
| 870-880 | 0.56 | 0.13 | 0.06 | 0.07 |
| 900-910 | 0.51 | 0.12 | 0.07 | 0.05 |

TABLE 2 C-N-S isotopes of core GC10.

| Depth (cmbsf) | $\delta^{13}C_{TIC}$ (V-PDB) | $\delta^{34}S$ (V-CDT) | $\delta^{15}N_{TN}$ (Air $N_2$) | $\delta^{15}N_{decarb}$ (Air $N_2$) | TS/TOC |
|---|---|---|---|---|---|
| 30-40 | 0.19 | 9.27 | 3.56 | 2.89 | 0.22 |
| 60-70 | 0.1 | 9.43 | 3.02 | 3.29 | 0.26 |
| 80-90 | -0.25 | 9.69 | 2.2 | 2.99 | 0.2 |
| 117-130 | 1.03 | -15.44 | 2.94 | 3.18 | 0.75 |
| 150-160 | 0.69 | -9.68 | 3.06 | 3.35 | 0.61 |
| 167-177 | 0.77 | -16.47 | 2.27 | 3.03 | 1.13 |
| 208-220 | 0.08 | -13.9 | 2.41 | 3.06 | 0.63 |
| 230-242 | 0.07 | -13.1 | 2.52 | 3.35 | 0.24 |
| 260-270 | 0.16 | -20.05 | 2.5 | 2.77 | 0.52 |
| 280-290 | 0 | -16.61 | 2.92 | 3.44 | 1.11 |
| 320-330 | -0.08 | -21.3 | 2.37 | 2.75 | 0.31 |
| 350-360 | -0.23 | -29.36 | 2.01 | 2.53 | 0.32 |
| 370-380 | -0.37 | -27.96 | 2.6 | 2.33 | 0.39 |
| 410-420 | 0.44 | -18.43 | 3.38 | 2.03 | 0.66 |
| 429-440 | -3.2 | -7.68 | 2.47 | 1.32 | 0.67 |
| 460-470 | -3.54 | -5.64 | 2.14 | 1.34 | 0.64 |
| 479-490 | -3.65 | -3.62 | 2.01 | 1.11 | 0.41 |
| 520-530 | -3.02 | 0.28 | 3.27 | 0.68 | 0.39 |
| 550-560 | -2.79 | -2.82 | 1.68 | 1.5 | 0.6 |
| 570-580 | -7.11 | -2.62 | 1.15 | 1.02 | 0.41 |
| 605-615 | -2.78 | -0.56 | 0.69 | 0.91 | 0.5 |
| 625-632 | -20.33 | -4.19 | 1.74 | 1.28 | 0.71 |
| 652-660 | -2.1 | -9.53 | 2.1 | 1.59 | 0.62 |
| 670-680 | -1.9 | -0.85 | 1.8 | 1.52 | 0.84 |
| 710-720 | -2.82 | 7.01 | 1.6 | 2.23 | 1.19 |
| 730-740 | -20.89 | 0.18 | 2.68 | 1.27 | 2.32 |
| 760-770 | -0.22 | 0.16 | 0.79 | 3.59 | 1.06 |
| 775-790 | -1.73 | -1.19 | 1.71 | 3.2 | 0.65 |
| 820-830 | -0.42 | 15.7 | 1.41 | 4.2 | 0.82 |
| 850-860 | -0.66 | 14.25 | 1.3 | 3.3 | 0.55 |
| 870-880 | -0.65 | 16.66 | 1.06 | 1.57 | 0.54 |
| 900-910 | -0.49 | 24.2 | 1.93 | 3.15 | 0.09 |

## 4.2 TOC, TN, $N_{decarb}$ and TS contents

The TN and $N_{decarb}$ content of sediment from site GC10 is presented in Figure 4A. The samples have TOC = 0.22–0.92 wt% (avg. 0.49 wt%; n = 32), TN = 0.08–0.2 wt% (avg. 0.13 wt%; n = 32), and $N_{decarb}$ = 0.03–0.11 wt% (avg. 0.07 wt%; n = 32). TOC, TN, and $N_{decarb}$ content display similar trends and vary widely. In 605–632 and 730-770 cmbsf, TOC, TN, and $N_{decarb}$ content present distinct decreases (Figure 4A, Table 1). The samples have TS = 0.04–0.79 wt% (avg. 0.29 wt%; n = 32). In 0-100 cmbsf, TS content displays relatively low values. In 100-560cmbsf, TS content is relatively high and varies widely. TS content shows a significant increase in 560–830 cmbsf (Figure 3C). TS/TOC is less than 0.36 in 0-100 cmbs and higher than 0.36 in 100-930 cmbsf (Figure 3B). TS/TOC displays a significant increase in 560-830 cmbsf.

## 4.3 TN and $N_{decarb}$ isotopes

The samples have $\delta^{15}N_{TN}$ = 0.69–3.56‰ (avg. 2.16‰; n = 32). In 0-100 cmbsf, the $\delta^{15}N_{TN}$ decreases with depth. In 100-560 cmbsf, the $\delta^{15}N_{TN}$ of sediment is relatively stable. The $\delta^{15}N_{TN}$ exhibits distinct negative excursions in 560-830 cmbsf. $\delta^{15}N_{decarb}$ varies from 0.68 to 4.20‰ (avg. 2.37‰; n = 32). In 0-100 cmbsf, the $\delta^{15}N_{decarb}$ of sediment is relatively stable. In 100-560 cmbsf, the $\delta^{15}N_{decarb}$ decreases with depth. The $\delta^{15}N_{decarb}$ shows positive excursion in 560–830 cmbsf (Figure 4, Table 2).

# 5 Discussion

## 5.1 Geological records for AOM

In order to reveal the nitrogen cycle in SMTZ, the SMTZ position of core GC10 must first be constrained. The current SMTZ of core GC10 has been constrained at ~800 cmbsf using porewater methane and sulfate concentrations (Wu et al., 2010). At ~800 cmbsf, methane concentrations rise sharply, whereas sulfate concentrations drop sharply with depth, indicative of the AOM occurrence there (Figures 2, 3). To trace the integral methane seepage dynamics, TS/TOC and the TIC and TS isotopes are also used here to trace the AOM geological record.

### 5.1.1 TS/TOC indicates AOM in sediment

In the marine sedimentary environment, sulfur comes primarily from pyrite ($FeS_2$), which is mainly sourced by sulfide from sulfate reduction of organic matter (OSR) and $Fe^{2+}$ from porewater (equations (5), (6), (7), and (8)), thus there is a dependency between the TS and TOC contents (Berner, 1984; Wang et al., 2018b). Because OSR would produce authigenic pyrite, the TS/TOC ratio is less than 0.36 in an oxic setting and larger than 0.36 in an anaerobic environment (Berner, 1984; Li et al., 2016). In the SMTZ, AOM produces additional authigenic pyrite (not dependent on TOC) (Berner, 1984; Li et al., 2016; Wang et al., 2018b), which significantly increases the sediment TS content and TS/TOC ratio (equations (4), (5), (6), (7), and (8)). Therefore, a high TS/TOC ratio is widely used to trace AOM in sediments (van Dongen et al., 2007; Li et al., 2018; Yang et al., 2020; Miao et al., 2021).

$$CH_4 + SO_4^{2-} \rightarrow HS^- + HCO_3^- + H_2O \quad (4)$$

$$2CH_2O + SO_4^{2-} \rightarrow H_2S + 2HCO_3^- \quad (5)$$

$$Fe^{2+} + HS^- \rightarrow FeS + H^+ \quad (6)$$

$$FeS + H_2S \rightarrow FeS_2 + H_2 \quad (7)$$

$$FeS + S_n^{2-} \rightarrow FeS_2 + S_{n-1}^{2-} \quad (8)$$

In core GC10, the TS/TOC ratio is< 0.36 in 0–100 cmbsf, which indicates that the horizon is oxidizing. Below 100 cmbsf, TS/TOC is generally > 0.36, indicative of an anaerobic environment. The sharp TS/TOC increase (reaching 2.32) in 560–830 cmbsf is most likely attributed to the presence of AOM-generated additional authigenic pyrite, thus constraining the SMTZ there (Figure 3B).

### 5.1.2 TIC isotopes trace authigenic carbonate generated by AOM

The TIC of bulk marine sediment is a mixture of different inorganic carbon sources (Yang et al., 2020). TIC is primarily derived from calcareous nannofossils and authigenic carbonate generated by the seawater dissolved inorganic carbon (DIC) pool ($\delta^{13}C$ = 0 ‰) (Suess, 2014; Consolaro et al., 2015). The carbon isotope composition of calcareous nannofossils varies from -2 to 2‰ in a marine sedimentary environment without methane leakage (Berger, 1970; Panieri et al., 2017), thus the TIC carbon isotope composition varies generally between -2 and 2‰ (Wang et al., 2018b; Feng et al., 2021b; Li et al., 2021). In methane leakage regions, the TIC of bulk marine sediment is composed of calcareous nannofossils and authigenic carbonate generated by special DIC pools (Meister et al., 2019). The potential DIC pools in the methane seepage region include AOM-derived DIC, OSR-derived DIC, and deep-DIC flux (Akam et al., 2020). AOM-derived DIC inherits the $^{13}C$ depletion from methane (biogenic methane $\delta^{13}C$ less than -50‰) (Peckmann et al., 1999; Peckmann et al., 2004; Peckmann et al., 2009). OSR-derived DIC inherits the $^{13}C$ depletion from organic matter ($\delta^{13}C$ of marine organic matter varies from -19 to -22‰) (Berner, 1978; Lim et al., 2011). Deep-DIC flux fluxes from methanogenic depths with higher $\delta^{13}C$ values (5 to 24‰) (Meister et al., 2019; Akam et al., 2020). In SMTZ, high alkalinity will convert

7-36% DIC pools into authigenic carbonate (Akam et al., 2020). These DIC pools convert to authigenic carbonate minerals in the sediments and/or overprint foraminiferal shells (Zhuang et al., 2016; Panieri et al., 2017; Bergamin et al., 2019), which significantly changes the TIC carbon isotope compositions of bulk marine sediment, causing TIC $^{13}C$ depletion. AOM-derived authigenic carbonate typically displays $^{13}C$ depletion (<−30‰) which mainly mirrors AOM-derived DIC. Because OSR-derived DIC is limited by the reactive organic matter content of sediment, OSR could only generate a small proportion of DIC (Consolaro et al., 2015; Beulig et al., 2017; Feng et al., 2018b; Li et al., 2018; Feng et al., 2021a; Li et al., 2021).

The $\delta^{13}C_{TIC}$ values show clear negative excursions in 560–830 cmbsf (reaching -20.89‰), which indicate a mixture of calcareous nannofossils and authigenic carbonate generated by the AOM-derived DIC pool (Figure 3D). AOM-induced negative excursions of $\delta^{13}C_{TIC}$ also been reported in many AOM-impacted sediment cores (Li et al., 2016; Xie et al., 2019; Hu et al., 2020; Xiong et al., 2020; Yang et al., 2020; Li et al., 2021). Therefore, the SMTZ was constrained at 560–830 cmbsf.

### 5.1.3 TS isotope reveals AOM impact on core GC10

Organic sulfur, elemental sulfur, and pyrite are all components of sulfur in marine sediment. Because organic sulfur, elemental sulfur, and Fe-sulfides are all metastable (Hofmann et al., 2009; Chen et al., 2016; Lin et al., 2016; Zhang et al., 2018), they are easily converted to pyrite. Pyrite is the most abundant sulfur component in bulk sediments (Berner, 1984). In an anaerobic marine environment, sulfate reduction bacteria preferentially use $^{32}S$ to generate pyrite when sulfate replenishment is sufficient (Hofmann et al., 2009; Chen et al., 2016; Lin et al., 2016; Zhang et al., 2018). Thus, the pyrite formed by organic matter sulfate reduction (OSR) is $^{34}S$-depleted (Borowski et al., 2013; Egger et al., 2015; Beulig et al., 2017). In SMTZ, the consumption rate of sulfates in interstitial water is much higher than the seawater sulfate replenishment rate, resulting in a residual $^{34}S$-rich sulfate pool, which eventually precipitates into $^{34}S$-rich pyrite *via* AOM (Borowski et al., 2013; Egger et al., 2015; Lin et al., 2016; Lin et al., 2018a). This will generate $^{34}S$-rich pyrite in marine sediment (Hofmann et al., 2009; Chen et al., 2016; Lin et al., 2016; Zhang et al., 2018). $\delta^{34}S_{TS}$ displays a similar tendency as $\delta^{34}S_{CRS}$, as pyrite is the major sulfur source in bulk sediment (Li et al., 2018; Liu et al., 2020; Feng et al., 2021b). $\delta^{34}S_{TS}$ can also indicate the sulfur isotope characteristic of pyrite (Wang et al., 2018b; Yang et al., 2020; Feng et al., 2021b).

In 0–100 cmbsf, $\delta^{34}S_{TS}$ is stable (from 9.27 to 9.69‰; avg. 9.46‰) and TS/TOC is< 0.36 (oxic zone), which were interpreted by disproportionation and reoxidation. Disproportionation and reoxidation of sulfide is most-likely attributed to heavy $^{34}S$ enrichment of pyrite in surface marine sediment (Lin et al., 2016; Lin et al., 2017). During very early diagenesis, there was an increased availability of easily degradable organic materials, which led to high cellular sulfate reduction rates and declining isotope discrimination (Lin et al., 2016; Lin et al., 2017). This is reflected in the high $\delta^{34}S$ values and low pyrite content (Lin et al., 2016; Lin et al., 2017). Such sulfide disproportionation and reoxidation (a high $\delta^{34}S$ value and a low pyrite content in shallow surface sediments) have been widely reported in surface sediment from continental margins and cold-seep regions (Borowski et al., 2013; Lin et al., 2017; Lin et al., 2018b). In 100–400 cmbsf, $\delta^{34}S$ decreases with depth and TS/TOC is high (> 0.36), which is most likely caused by the addition of OSR-driven $^{34}S$-depleted pyrite. In 100-400 cmbsf, OSR is occurring due to the anoxic environment (TS/TOC > 0.36). The rate of OSR is slow enough not to contribute to a sulfate gradient, but strong enough to produce enough isotopically light sulfide in here. It is indicated by the $\delta^{34}S$ decrease with depth in 100-400 cmbsf but sulfate concentration is relatively stable. The negative $\delta^{34}S$ value of pyrite generated by OSR is also reported in most marine sediments (Berner, 1978; Robinson et al., 2012; Borowski et al., 2013; Li et al., 2016; Lin et al., 2016; Antler et al., 2017; Lin et al., 2018a; Lin et al., 2018b; Lin et al., 2021; Lin et al., 2021). In 400–830 cmbsf, $\delta^{34}S$ increases with depth (Figure 3D), which is most likely due to AOM-generated $^{34}S$-rich pyrite. The positive excursion of $\delta^{34}S$ below the SMTZ (below 830 cmbsf) is most likely caused by the sulfate reduction rate faster than the sulfate replenish rate (Liu et al., 2020). This phenomenon was also observed in many sediment cores in the Bornholm Basin (Liu et al., 2020).

In a word, the SMTZ of GC10 are restricted at 560–830 cmbsf, based on a significantly increased TS/TOC ratio, $\delta^{13}C_{TIC}$ negative excursions, $\delta^{34}S$ positive excursions, and methane/sulfate concentration.

## 5.2 Nitrogen geochemistry and its constraints for nitrogen cycle in SMTZ

### 5.2.1 Nitrogen geochemistry in interstitial water

We compiled $NH_4^+$, methane, and sulfate concentrations from Wu et al. (2010) to reflect the nitrogen cycle and biochemical rate (Wu et al., 2010). In the core of GC10, $NH_4^+$ concentration rises with depth and then falls sharply to the current SMTZ, below which it rises sharply again (Figure 2D). $NH_4^+$ is a major nitrogen component in interstitial water that is mostly released by organic matter degradation (Laima, 1992; Yang et al., 2010). $NH_4^+$, as an indicator of organic matter degradation, has been utilized in many continental margin porewater investigations (Nakatsuka et al., 1997; Holmes et al., 1999; Freudenthal et al., 2001; Wehrmann et al., 2011; Robinson et al., 2012; Schrum et al., 2015; Komada et al., 2016). The concentration of $NH_4^+$ in pore water normally increases with

depth in a marine environment without methane seepage, which has been interpreted as organic matter degradation releasing $NH_4^+$ accumulation in interstitial water (Lehmann et al., 2007; Wehrmann et al., 2011; Robinson et al., 2012; Quan et al., 2013a; Tesdal et al., 2013; Schrum et al., 2015; Akam et al., 2020; Zhang et al., 2021). The laboratory incubation found that organic matter decomposition releases $NH_4^+$, and $NH_4^+$ concentration increases with incubation time (Holmes et al., 1999; Freudenthal et al., 2001; Lehmann et al., 2002; Wehrmann et al., 2011). The age of organic matter in marine sediment increases with depth, thus $NH_4^+$ concentration increases with depth in normal marine environment (Nakatsuka et al., 1997; Holmes et al., 1999; Freudenthal et al., 2001; Wehrmann et al., 2011; Robinson et al., 2012; Schrum et al., 2015; Komada et al., 2016).

In the methane seepage region, the $NH_4^+$ concentration increases from low values near the seafloor to an interval where the concentration gradients are minimal, followed by a pronounced increase very close to the depth where sulfate values approach zero (Wehrmann et al., 2011; Schrum et al., 2015). In fact, the zone where sulfate values approach zero coincides with the SMTZ lower boundary. Therefore, in the methane seepage region, the $NH_4^+$ concentration increases with depth, and the concentration gradients are minor in the SMTZ but significantly higher below the SMTZ. The concentration gradients are minimal in the SMTZ, which is interpreted by sulfate-reducing ammonium oxidation and ammonia assimilation into biomass (Wehrmann et al., 2011; Schrum et al., 2015). Sulfate-reducing ammonium oxidation (SRAO) could be illustrated as equation (10) (Schrum et al., 2015). According to computed Gibbs energies, sulfate-reducing ammonium oxidation is energy yielding and metabolically practical (Schrum et al., 2015). The rapid increase in $NH_4^+$ concentration below SMTZ is interpreted by the upward $NH_4^+$ flow carried by methane leakage (Wehrmann et al., 2011; Schrum et al., 2015).

$$4NH_4^+ + 4SO_4^{2-} + 5(CH_2O)_n \rightarrow 5CO_2 + 2N_2 + 11H_2O + 4HS^- \quad (10)$$

The whole down-core profile of $NH_4^+$ concentration for GC10 is similar to most AOM-impacted sediment cores from the Bering Sea Slope, Bay of Bengal and Greenwich Bay (Wehrmann et al., 2011; Schrum et al., 2015). In the oxidation zone of 0-100 cmbsf (TS/TOC< 0.36), the $NH_4^+$ concentration was stabilized at a low value (average 46.1 μmol/L) most likely due to the release of $NH_4^+$ from organic matter degradation under oxidative conditions. Organic matter could be degraded by $O_2$, N, Fe, Mn, and $SO_4^{2-}$; it depends on the Gibbs energy difference ($O_2$ < Mn < N < Fe < $SO_4^{2-}$) (Froelich et al., 1979; Thullner et al., 2007; LaRowe and Van Cappellen, 2011). The lower the Gibbs energy, the more likely the reaction is to happen (Froelich et al., 1979; Thullner et al., 2007; LaRowe and Van Cappellen, 2011). In 0-100 cmbsf, TS/TOC is less than 0.36, indicating an oxidation condition. Because the Gibbs energy of organic matter degradation by $O_2$ is lower than that of $SO_4^{2-}$, most organic matter is degraded by $O_2$ in 0-100 cmbsf. The concentration of $NH_4^+$ increases with depth in the range of 100-560 cmbsf, which is most likely owing to organic matter age increasing with depth and interstitial water accumulating $NH_4^+$ produced by organic matter decomposition. In 100-560 cmbsf, TS/TOC is higher than 0.36, indicating an anaerobic condition. Thus, in 100-560 cmbsf, most organic matter is degraded by $SO_4^{2-}$. The SMTZ (560-830 cmbsf) has a lower $NH_4^+$ concentration, which is most likely due to $NH_4^+$ consumption by the SRAO. Below the SMTZ (830-930 cmbsf), $NH_4^+$ concentration increases sharply (reach to 367.9 μmol/L), accounting for deep $NH_4^+$ flux upward with methane leakage.

Based on above mentioned, $NH_4^+$ concentration decreases in the SMTZ which most likely indicate sulfate-reducing ammonium oxidation occurrence there.

### 5.2.2 Nitrogen geochemistry in marine sediment

In marine sediment, the potential nitrogen sources include nitrogen from particulate organic matter, nitrogen from dissolved organic matter, $NO_3^-$, exchangeable $NH_4^+$, and $NH_4^+$ fixed into clay mineral structures (Macko and Estep, 1984; Karl et al., 1997; Holmes et al., 1999; Lehmann et al., 2007; Martens-Habbena and Qin, 2022). The most abundant nitrogen source in marine sediment is nitrogen from organic matter (Karl et al., 1997; Hong et al., 2013; Tesdal et al., 2013; Komada et al., 2016; Kuypers et al., 2018). Exchangeable $NH_4^+$ makes up only a modest percentage of nitrogen (<1%) in open ocean sediments with little TOC, but its content will rise in anaerobic environments as interstitial water $NH_4^+$ concentrations rise and the significant capacity of the clays to absorb $NH_4^+$ (Freudenthal et al., 2001; Lehmann et al., 2007; Robinson et al., 2012; Hong et al., 2013; Schrum et al., 2015; Martens-Habbena and Qin, 2022). $NH_4^+$ fixed into clay mineral structures would be a substantial nitrogen pool in marine sediment with low organic matter content, but in environments with high organic matter content, the main nitrogen pool is nitrogen from organic matter (Alshameri et al., 2018).

TN, $N_{decarb}$, and $N_{other}$ contents are illustrated in Figure 4A. Interesting, TN, $N_{decarb}$, and $N_{other}$ content display distinct drops in 625-632 and 730-740 cmbsf, which are most likely due to AOM-generating carbonate diluting nitrogen content in sediment. Because $\delta^{13}C_{TIC}$ displays negative excursions in 625-632 and 730-740 cmbsf, indicating that AOM generates a substantial amount of carbonate there. In 625-632 cmbsf, $N_{decarb}$ content even higher than TN content, which also consistent with that carbonate dilute nitrogen content in sediment there. Thus, TN, $N_{decarb}$ and $N_{other}$ contents could be influenced by carbonate dilution and could not reflect nitrogen accumulation.

TN is made up of $N_{decarb}$, and $N_{other}$ in this study. The nitrogen sources of marine sediment associated with different nitrogen types are depicted in Figure 5. PON, DON, E-AM, $NO_3^-$, and CFN are all possible nitrogen types for TN. The probable

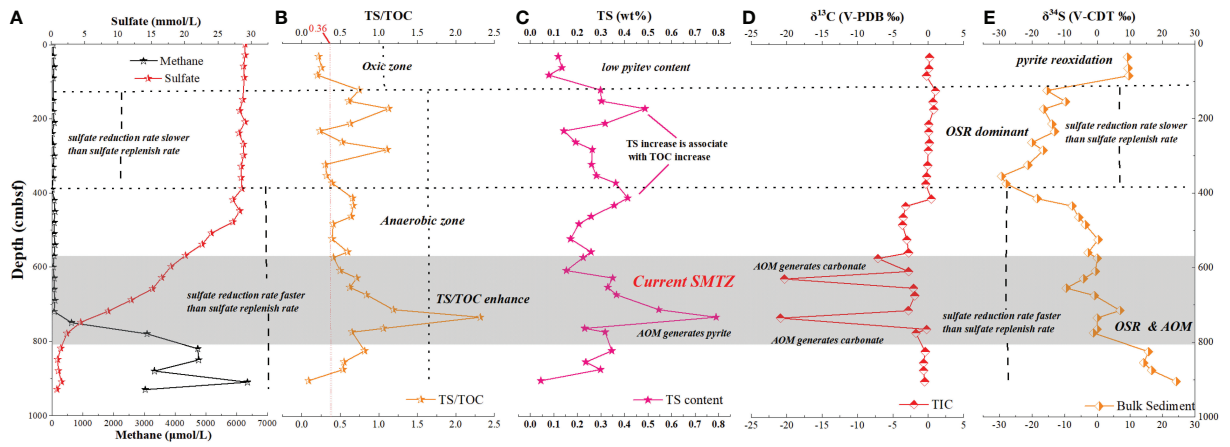


FIGURE 3
Geological records of SMTZ in core GC10. **(A)** Interstitial water data for GC10 (Wu et al., 2010). Methane concentrations rise, and sulfate drops sharply at 560–830 cmbsf, indicating the SMTZ location there. **(B)** TS/TOC of sediments from GC10. TS/TOC enhances at 560–830 cmbsf. **(C)** Total sulfur content for GC10. Total surfur content increases at 560-830 cmbsf, indicating additional pyrite generated by AOM. **(D)** Total inorganic carbon δ13C for sediments, showing negative δ13CTIC excursions at 560–830 cmbsf (reaching -20.89‰), and indicating AOM occurrence here. **(E)** Bulk-sediment δ34S for GC10. δ34S values are positive in 0–100 cmbsf, decrease in 100-400 cmbsf, and variably increase in 400–937 cmbsf.

nitrogen types of $N_{decarb}$ include PON and CFN, while DON, $NO_3^-$ and E-AM are all potential types for $N_{other}$. E-AM and CFN may not be the majority nitrogen types at site GC10, because site GC10 is a typical methane seep location with substantial organic matter (average TOC content = 0.49 wt%). The majority of nitrogen in GC10 is related to organic matter, since TOC vs TN and TOC vs $N_{decarb}$ in GC10 show a clear positive correlation (Figure 6). This implies that TN and $N_{decarb}$ of sediment in site GC10 are mostly derived from organic matter.

The $\delta^{15}N$ of organic matter is controlled by sedimentary input and early diagenesis (Lehmann et al., 2002; Komada et al., 2016; Chuang et al., 2019; Zhang et al., 2020). a) Sedimentary input. Nitrogen isotopes from various organic matter sources would have varying $\delta^{15}N$ values (Nakatsuka et al., 1997; Freudenthal et al., 2001; Lehmann et al., 2007; Reeburgh, 2007; Robinson et al., 2012). Organic matter $\delta^{15}N$ would vary with different sedimentary inputs. Organic matter would have little $\delta^{15}N$ offset in an area with steady sedimentary input (relatively

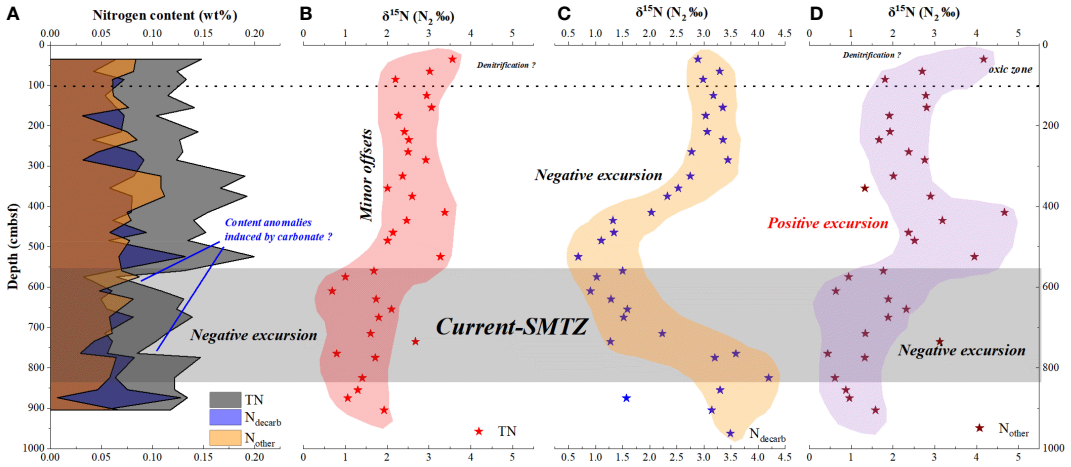


FIGURE 4
Element and isotope compositions of different nitrogen species for GC10. δ15NTN and δ15Nother shows negative excursions in the SMTZ. **(A)** TN, Ndecarb and Nother content;**(B)** TN isotope; **(C)** Ndecarb isotope; **(D)** Nother isotope.

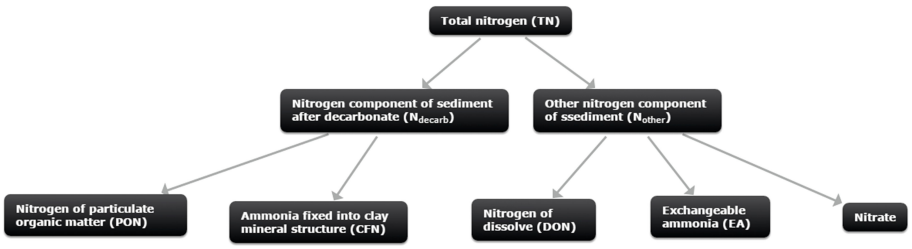


FIGURE 5
Nitrogen composition of marine sediment. Total nitrogen (TN) includes $N_{decarb}$ and $N_{other}$; $N_{decarb}$ includes nitrogen of particulate organic matter (PON) and amminia fixed into clay minerals structure (CFN); $N_{other}$ includes nitrogen of dissolve organic matter (DON) and exchangeable ammonia, and negligeble nitrate.

stable organic matter source and relatively stable sedimentation rate). b) Early diagenesis. In early diagenesis, a variety of aerobic and anaerobic microbial processes could modify the $\delta^{15}N$ of organic matter (nitrate utilization, denitrification, nitrification, $N_2$-fixation, organic matter degradation, and sulfate-reducing ammonium oxidation) (Macko and Estep, 1984; Robinson et al., 2012; Komada et al., 2016; Wang et al., 2018a; Akam et al., 2020).

Nitrate utilization, denitrification, and nitrification are all associated with nitrate. Although nitrate utilization and denitrification can result in large nitrogen isotope fractionation (up to 30‰), nitrate is exhausted by denitrification within a few centimeters (Lehmann et al., 2007). Below the seafloor, in anaerobic environment, low nitrate concentration in deep sediment can lead to under-expression of this isotope effect, both at the organism and sediment scales (Lehmann et al., 2007). Thus, the $\delta^{15}N$ of organic matter in deep sediment is less impacted by nitrate utilization, denitrification, and nitrification. $N_2$-fixation may also result in a negative excursion of sediment $\delta^{15}N$ (Karl et al., 1997), as $N_2$ has a relatively low nitrogen isotope ($\delta^{15}N$ = 0‰) (Robinson et al., 2012). ANME is a type of $N_2$-fixation diazotrophic bacteria (Dekas et al., 2009), which could result in the depletion of $^{15}N$ in sediment (Hu et al., 2020). Organic matter degradation could also modify the nitrogen isotope of sediment (Nakatsuka et al., 1997; Holmes et al., 1999; Freudenthal et al., 2001; Lehmann et al., 2002; Lehmann et al., 2007). Selective loss of specific fractions from total organic matter during degradation could alter the $\delta^{15}N$ of organic matter (Libes and Deuser, 1988; Karl et al., 1997; Nakatsuka et al., 1997; Komada et al., 2016; Meister et al., 2019). Carbohydrates, proteins, and lipids make up organic matter in marine sediment, and degradation of organic matter can change the relative abundance of carbohydrates, proteins, and lipids (Karl et al., 1997; Robinson et al., 2012). This could also change the nitrogen isotope component of organic matter (Karl et al., 1997; Robinson et al., 2012). Organic matter degradation preferential degradation of amino acids ($^{15}N$-rich) (Nakatsuka et al., 1997) and selective removal of proteins (with relative $^{15}N$ rich) (Macko and Estep, 1984) which could induce $\delta^{15}N$ of organic matter negative excursion.

The $\delta^{15}N_{TN}$ of sediment displays a relatively high value in 0-100 cmbsf, shows relatively stable values (offset 2‰) in 100-530 cmbsf, and displays a negative excursion in the SMTZ. In 0-100 cmbsf, the $\delta^{15}N_{TN}$ of sediment displays a relatively high value, which is most likely due to denitrification. In an oxic condition, denitrification would make surface marine sediment $^{15}N$ enriched (Lehmann et al., 2007). In 0-100 cmbsf, TS/TOC<0.36 indicates an oxic environment here, which favors denitrification and sediment $^{15}N$ enrichment. In 100-530 cmbsf, the $\delta^{15}N_{TN}$ between the fluff layers is relatively steady (Figure 4B), which reflects relatively stable sedimentary input in site GC10. In addition, the nitrogen isotope of sediment from northern South China Sea (site MD3433, that study site is close to our study area) is relatively stable (< 1‰) since 50 ka (Figure 1) (Wang et al., 2018a), which consistent with site GC10 has relatively stable sedimentary input. *In the SMTZ (560-830 cmbsf), the* $\delta^{15}N_{TN}$ of sediment displays a negative excursion, which is most likely due to nitrogen uptake by ANME or AOM microbial consortiums. The $\delta^{15}N_{TN}$ of sediment cores displaying negative excursions in AOM-impacted zones has been observed in many methane seepage regions (Hu et al., 2020). This phenomenon is interpreted by the nitrogen uptake of ANME or AOM microbial consortiums (Hu et al., 2020). However, the nitrogen source in SMTZ is not well understood. Combining with SRAO would consume $NH_4^+$ and produce $N_2$ (equation 10) in the SMTZ, the negative excursion of $\delta^{15}N_{TN}$ in the SMTZ likely due to that $N_2$ generated by SRAO was fixed into marine sediment. There are further studies needed to confirm it.

Interestingly, $\delta^{15}N_{decarb}$ displays a different tendency from $\delta^{15}N_{TN}$.The $\delta^{15}N_{decarb}$ of sediment decreases with depth in 0-530 cmbsf and displays a positive excursion in the SMTZ. In 0-530 cmbsf, the $\delta^{15}N_{decarb}$ of sediment decreases with depth, which is most likely due to organic matter degradation. Organic matter degradation would consume organic matter and release $NH_4^+$ (Nakatsuka et al., 1997). Organic matter degradation involves preferential degradation of amino acids and selective removal of proteins (with relative $^{15}N$ rich) (Macko and Estep, 1984), which

would induce the $\delta^{15}N$ of particular organic matter decrease. In 0-530 cmbsf, the $\delta^{15}N_{decarb}$ decrease with depth, and $NH_4^+$ concentration increase with depth, which are consistent with organic matter degradation releasing $NH_4^+$ and inducing $\delta^{15}N_{decarb}$ decrease. The plot of $\delta^{15}N_{decarb}$ vs $NH_4^+$ displays a negative correlation (Figure 6B), which is also consistent with it. In the SMTZ, the $\delta^{15}N_{decarb}$ of sediment displays a positive excursion, which is likely due to the organic matter degradation rate decreasing in the SMTZ. In SMTZ, methane competes with organic matter for becoming the substrate of *Sulfate Reduction Bacteria* (Jørgensen et al., 2019), which would decrease the organic matter degradation rate. The AOM rate, methanogenesis rate, and POC (particulate organic carbon) degradation rate are estimated, based on interstitial water *via* numerical simulation calculation. In GC10, the low POC degradation rate in the SMTZ is consistent with $\delta^{15}N_{decarb}$ positive excursion that is possible due to the organic matter degradation rate decrease in the SMTZ.

TN is a mixture of $N_{decarb}$ and $N_{other}$. TN is derived from both particulate organic matter and soluble organic matter. $N_{decarb}$ only comes from particulate organic matter. The $\delta^{15}N_{decarb}$ of sediment is mainly controlled by organic matter degradation, but the $\delta^{15}N_{TN}$ of sediment reflects the nitrogen fixation and ammonia assimilation influence of ANME/AOM microbial consortiums. This indicates that the nitrogen fixation process and ammonia assimilation of ANME may mainly control the soluble organic nitrogen isotope composition. The calculated $\delta^{15}N_{other}$ shows negative excursions in the SMTZ, which further supports our opinion (Figure 4A). In addition, $N_2$-fixation induced negative excursion of soluble organic matter $\delta^{15}N$ has been reported in many studies (Karl et al., 1997; Robinson et al., 2012).

### 5.2.3 Nitrogen cycle model in the SMTZ

Based on $\delta^{15}N_{TN}$, $\delta^{15}N_{decarb}$, TOC content, and $NH_4^+$ concentration of core GC10, we present a nitrogen cycle model in SMTZ, which is depicted in Figure 7. When SMTZ is positioned in the sediment column, as an anaerobic environment, nitrate will be quickly consumed by denitrification at the sediment surface, and nitrate is absent from the nitrogen cycle in SMTZ. The nitrogen cycle in SMTZ will only be associated with $NH_4^+$ in interstitial water, nitrogen in sediment, and $N_2$.

Sulfate-reducing ammonium oxidation (SRAO) would consume $NH_4^+$ and release $N_2$ in SMTZ (Schrum et al., 2015). This would induce a decrease in $NH_4^+$ concentration and an increase in $N_2$ concentration. In SMTZ, as abundant ANME could mediate $N_2$-fixation (Boetius et al., 2000; Boetius and Wenzhöfer, 2013; Suess, 2014; Feng et al., 2015; Feng et al., 2018b; Suess, 2020), $N_2$-fixation rate clearly increased. Diazotrophic bacteria (ANME is one of them) mediating $N_2$-fixation would cause a decrease in the soluble nitrogen isotope (Karl et al., 1997; Robinson et al., 2012). $N_2$ released from SRAO would be fixed into sediment *via* soluble organic matter due to ANME $N_2$-fixation. Because $N_2$ has a relatively lighter nitrogen isotope ($\delta^{15}N \approx 0$ ‰), the $\delta^{15}N_{TN}$ of sediment would exhibit negative excursion in SMTZ. As to the $\delta^{15}N_{decarb}$ of sediment, it is controlled by organic matter degradation. In SMTZ, methane competes with organic matter, which induce organic matter degradation rate decrease and the $\delta^{15}N_{decarb}$ of sediment displays a positive excursion. This nitrogen cycle model could be modified in the future as more research on the nitrogen cycle in SMTZ is conducted. This study shows that the unique geochemistry processes in SMTZ would modify the nitrogen geochemistry characteristics.

## 6 Conclusions

(1) Based on the TIC and TS isotopes, TS/TOC, methane and sulfate concentrations of the sediment core GC10

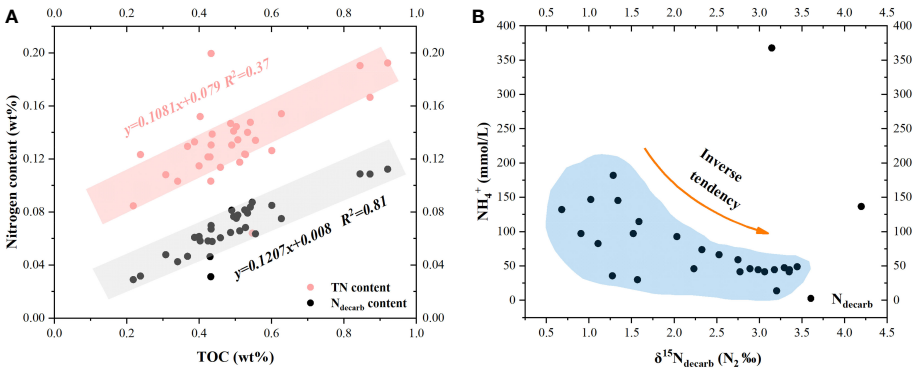


FIGURE 6
Scatter plot for nitrogen contents and isotopes of GC10. TN and $N_{decarb}$ contents increase with TOC content, indicating that nitrogen in sediments mainly comes from organic matter. **(A)** Scatter plots for TOC vs TN and TOC vs $N_{decarb}$. **(B)** Scatter plot for $NH_4^+$ vs $\delta^{15}N_{decarb}$.

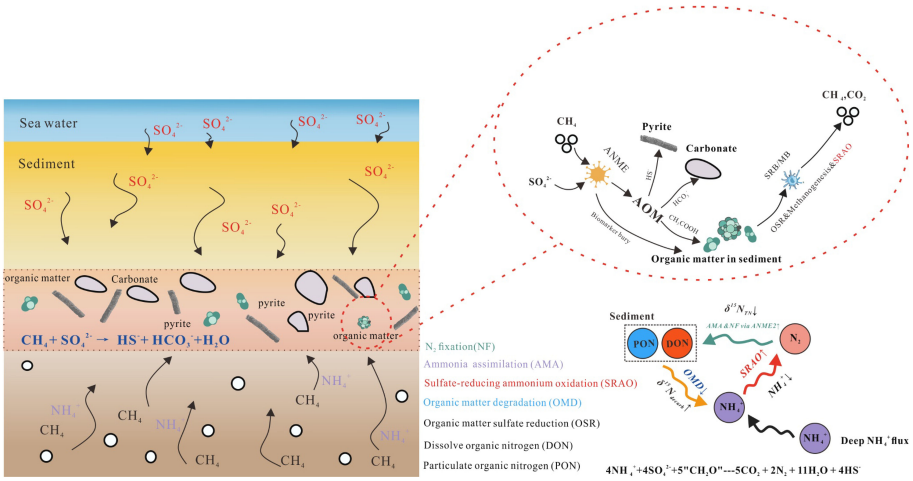


FIGURE 7
Schematic diagram for the nitrogen cycle in SMTZ. The nitrogen cycle in SMTZ is connected with nitrogen in sediment, $NH_4^+$ in porewater, and $N_2$ in air. As sulfate-reducing ammonium oxidation (SRAO) would consume $NH_4^+$, $NH_4^+$ concentration will decrease in SMTZ. Because ANME is most abundant in SMTZ, the rate of $N_2$-fixation (mediated by ANME) rises. The dissolve organic nitrogen isotope will decrease as a result of $N_2$-fixation (ANME mediate), and the $\delta^{15}N_{TN}$ of sediment display negative excursion in SMTZ.

from the southwestern Taiwan basin (South China Sea), the current SMTZ is delineated at 560–830 cmbsf.

(2) In the SMTZ, $NH_4^+$ concentration decreases due to sulfate-reducing ammonium oxidation. Below the current SMTZ, $NH_4^+$ concentration increases sharply due to the upward deep- $NH_4^+$ flux.

(3) The $\delta^{15}N_{decarb}$ variation in core GC10 is most likely due to organic matter degradation. The $\delta^{15}N_{TN}$ displays distinct negative excursions in the SMTZ, which are interpreted as ANME $N_2$-fixation modifying the soluble nitrogen isotope.

(4) The nitrogen isotope of sediment would experience a negative excursion in SMTZ is most likely due to the release of $N_2$ caused by sulfate-reducing ammonium oxidation and the regulation of $N_2$ fixing there by abundant ANME.

## Data availability statement

The original contributions presented in the study are included in the article/Supplementary Material. Further inquiries can be directed to the corresponding authors.

## Author contributions

XY: Wrote the manuscript. YZ: Analysis of N isotopes. XS: Supervision of the project. LX: Analysis and interpretation of data. TC: Analysis if N content. All authors contributed to the article and approved the submitted version.

## Funding

This research was jointly funded by the Natural Science Foundation of China (41876038, 91128101, 41806049) and the Guangdong Special Fund for Economic Development (Marine Economy, GDME-2018D001).

## Acknowledgments

We are grateful to Dr. Hongfeng Lu and the Guangzhou Marine Geological Survey for providing samples and valuable suggestions.

## Conflict of interest

The authors declare that they have no known competing financial interests or personal relationships that could have appeared to influence the work reported in this paper.

## Publisher's note

All claims expressed in this article are solely those of the authors and do not necessarily represent those of their

affiliated organizations, or those of the publisher, the editors and the reviewers. Any product that may be evaluated in this article, or claim that may be made by its manufacturer, is not guaranteed or endorsed by the publisher.

## Supplementary material

The Supplementary Material for this article can be found online at: https://www.frontiersin.org/articles/10.3389/fmars.2022.1101599/full#supplementary-material

## References

Akam, S. A., Coffin, R. B., Abdulla, H. A. N., and Lyons, T. W. (2020). Dissolved inorganic carbon pump in methane-charged shallow marine sediments: State of the art and new model perspectives. *Front. Mar. Sci.* 7. doi: 10.3389/fmars.2020.00206

Alshameri, A., He, H., Zhu, J., Xi, Y., Zhu, R., Ma, L., et al. (2018). Adsorption of ammonium by different natural clay minerals: Characterization, kinetics and adsorption isotherms. *Appl. Clay Sci.* 159, 83–93. doi: 10.1016/j.clay.2017.11.007

Antler, G., Turchyn, A. V., Herut, B., and Sivan, O. (2015). A unique isotopic fingerprint of sulfate-driven anaerobic oxidation of methane. *Geology* 43, 619–622. doi: 10.1130/G36688.1

Antler, G., Turchyn, A. V., Ono, S., Sivan, O., and Bosak, T. (2017). Combined 34S, 33S and 18O isotope fractionations record different intracellular steps of microbial sulfate reduction. *Geochim. Cosmochim. Acta* 203, 364–380. doi: 10.1016/j.gca.2017.01.015

Bergamin, L., Di Bella, L., Ferraro, L., Frezza, V., Pierfranceschi, G., and Romano, E. (2019). Benthic foraminifera in a coastal marine area of the eastern ligurian Sea (Italy): Response to environmental stress. *Ecol. Indic.* 96, 16–31. doi: 10.1016/j.ecolind.2018.08.050

Berger, W. H. (1970). Planktonic foraminifera: Selective solution and the lysocline. *Mar. Geol.* 8, 111–138. doi: 10.1016/0025-3227(70)90001-0

Berner, R. A. (1978). Sulfate reduction and the rate of deposition of marine sediments. *Earth Planet. Sci. Lett.* 39, 308. doi: 10.1016/0012-821x(78)90209-1

Berner, R. A. (1984). Sedimentary pyrite formation: An update. *Geochim. Cosmochim. Acta* 48, 605–615. doi: 10.1016/0016-7037(84)90089-9

Beulig, F., Røy, H., Glombitza, C., and Jørgensen, B. B. (2017). Control on rate and pathway of anaerobic organic carbon degradation in the seabed. *Proc. Natl. Acad. Sci. U. S. A.* 115, 367–372. doi: 10.1073/pnas.1715789115

Boetius, A., Ravenschlag, K., Schubert, C. J., Rickert, D., Widdel, F., Gleseke, A., et al. (2000). A marine microbial consortium apparently mediating anaerobic oxidation methane. *Nature* 407, 623–626. doi: 10.1038/35036572

Boetius, A., and Wenzhöfer, F. (2013). Seafloor oxygen consumption fuelled by methane from cold seeps. *Nat. Geosci.* 6, 725–734. doi: 10.1038/ngeo1926

Borowski, W. S., Paull, C. K., and Ussler, W. (1996). Marine pore-water sulfate profiles indicate *in situ* methane flux from underlying gas hydrate. *Geology* 24, 655–658. doi: 10.1130/0091-7613(1996)024<0655:MPWSPI>2.3.CO;2

Borowski, W. S., Rodriguez, N. M., Paull, C. K., and Ussler, W. (2013). Are 34S-enriched authigenic sulfide minerals a proxy for elevated methane flux and gas hydrates in the geologic record? *Mar. Pet. Geol.* 43, 381–395. doi: 10.1016/j.marpetgeo.2012.12.009

Chen, F., Hu, Y., Feng, D., Zhang, X., Cheng, S., Cao, J., et al. (2016). Evidence of intense methane seepages from molybdenum enrichments in gas hydrate-bearing sediments of the northern south China Sea. *Chem. Geol.* 443, 173–181. doi: 10.1016/j.chemgeo.2016.09.029

Chuang, P. C., Yang, T. F., Wallmann, K., Matsumoto, R., Hu, C. Y., Chen, H. W., et al. (2019). Carbon isotope exchange during anaerobic oxidation of methane (AOM) in sediments of the northeastern south China Sea. *Geochim. Cosmochim. Acta* 246, 138–155. doi: 10.1016/j.gca.2018.11.003

Clennell, M., Hovland, M., Booth, J., Hwnry, P., and Winters, W. (1999). Formation of natural gas hydrates in marine sediments: Gas hydrate growth and stability conditioned by host sediment properties. *J. Geophys. Res.* 104, 22,985–23,003. doi: 10.1111/j.1749-6632.2000.tb06842.x

Consolaro, C., Rasmussen, T. L., Panieri, G., Mienert, J., Bünz, S., and Sztybor, K. (2015). Carbon isotope (d13C) excursions suggest times of major methane release during the last 14 kyr in fram strait, the deep-water gateway to the Arctic. *Clim. Past* 11, 669–685. doi: 10.5194/cp-11-669-2015

Dekas, A. E., Poretsky, R. S., and Orphan, V. J. (2009). Deep-Sea archaea fix and share nitrogen in methane-consuming microbial consortia. *Science* 326, 422–426. doi: 10.1126/science.1178223

Dickens, G. R. (2003). Rethinking the global carbon cycle with a large, dynamic and microbially mediated gas hydrate capacitor. *Earth Planet. Sci. Lett.* 213, 169–183. doi: 10.1016/S0012-821X(03)00325-X

Dong, F., Peng, Y., Peckmann, J., Roberts, H., and Duofu, C. (2017). Stable carbon, nitrogen and sulfur isotopes in non-carbonate fractions of cold-seep carbonates. *Geophys. Res. Abstr.* 19, 3402. doi: 10.1130/G38233.1

Egger, M., Rasigraf, O., Sapart, C. J., Jilbert, T., Jetten, M. S. M., Röckmann, T., et al. (2015). Iron-mediated anaerobic oxidation of methane in brackish coastal sediments. *Environ. Sci. Technol.* 49, 277–283. doi: 10.1021/es503663z

Egger, M., Riedinger, N., Mogollón, J. M., and Jørgensen, B. B. (2018). Global diffusive fluxes of methane in marine sediments. *Nat. Geosci.* 11, 421–425. doi: 10.1038/s41561-018-0122-8

Ettwig, K. F., Butler, M. K., Le Paslier, D., Pelletier, E., Mangenot, S., Kuypers, M. M. M., et al. (2010). Nitrite-driven anaerobic methane oxidation by oxygenic bacteria. *Nature* 464, 543–548. doi: 10.1038/nature08883

Feng, D., Cheng, M., Kiel, S., Qiu, J. W., Yang, Q., Zhou, H., et al. (2015). Using bathymodiolus tissue stable carbon, nitrogen and sulfur isotopes to infer biogeochemical process at a cold seep in the south China Sea. *Deep. Res. Part I Oceanogr. Res. Pap.* 104, 52–59. doi: 10.1016/j.dsr.2015.06.011

Feng, J., Li, N., Liang, J., Shang, J., Yang, S., and Wang, H. (2021b). Using multi-proxy approach to constrain temporal variations of methane flux in methane-rich sediments of the southern south China Sea. *Mar. Pet. Geol.* 132, 105152. doi: 10.1016/j.marpetgeo.2021.105152

Feng, D., Peckmann, J., Li, N., Kiel, S., Qiu, J. W., Liang, Q., et al. (2018a). The stable isotope fingerprint of chemosymbiosis in the shell organic matrix of seep-dwelling bivalves. *Chem. Geol.* 479, 241–250. doi: 10.1016/j.chemgeo.2018.01.015

Feng, D., Pohlman, J. W., Peckmann, J., Sun, Y., Hu, Y., Roberts, H. H., et al. (2021a). Contribution of deep-sourced carbon from hydrocarbon seeps to sedimentary organic carbon: Evidence from radiocarbon and stable isotope geochemistry. *Chem. Geol.* 585, 120572. doi: 10.1016/j.chemgeo.2021.120572

Feng, D., Qiu, J. W., Hu, Y., Peckmann, J., Guan, H., Tong, H., et al. (2018b). Cold seep systems in the south China Sea: An overview. *J. Asian Earth Sci.* 168, 3–16. doi: 10.1016/j.jseaes.2018.09.021

Freudenthal, T., Wagner, T., Wenzhöfer, F., Zabel, M., and Wefer, G. (2001). Early diagenesis of organic matter from sediments of the Eastern subtropical Atlantic: Evidence from stable nitrogen and carbon isotopes. *Geochim. Cosmochim. Acta* 65, 1795–1808. doi: 10.1016/S0016-7037(01)00554-3

Froelich, P. N., Klinkhammer, G. P., Bender, M. L., Luedtke, N. A., Heath, G. R., Cullen, D., et al. (1979). Early oxidation of organic matter in pelagic sediments of the eastern equatorial Atlantic: suboxic diagenesis. *Geochim. Cosmochim. Acta* 43, 1075–1090. doi: 10.1016/0016-7037(79)90095-4

Hofmann, A., Bekker, A., Rouxel, O., Rumble, D., and Master, S. (2009). Multiple sulphur and iron isotope composition of detrital pyrite in archaean sedimentary rocks: A new tool for provenance analysis. *Earth Planet. Sci. Lett.* 286, 436–445. doi: 10.1016/j.epsl.2009.07.008

Holmes, M. E., Eichner, C., Struck, U., and Wefer, G. (1999). Reconstruction of surface ocean nitrate utilization using stable nitrogen isotopes in sinking particles and sediments. *Use Proxies Paleoceanogr.* 40, 447–468. doi: 10.1007/978-3-642-58646-0_18

Hong, W. L., Torres, M. E., Kim, J. H., Choi, J., and Bahk, J. J. (2013). Carbon cycling within the sulfate-methane-transition-zone in marine sediments from the ulleung basin. *Biogeochemistry* 115, 129–148. doi: 10.1007/s10533-012-9824-y

Hu, Y., Feng, D., Peng, Y., Peckmann, J., Kasten, S., Wang, X., et al. (2020). A prominent isotopic fingerprint of nitrogen uptake by anaerobic methanotrophic archaea. *Chem. Geol* 558, 119972. doi: 10.1016/j.chemgeo.2020.119972

Group I, Averyt, M, Solomon, S, et al (2007). IPCC, Climate Change : The Physical Science Basis. South African Geographical Journal Being A Record of the Proceedings of the South African Geographical Society. 92, 86–87. doi: 10.1080/03736245.2010.480842

Jørgensen, B. B., Beulig, F., Egger, M., Petro, C., Scholze, C., and Røy, H. (2019). Organoclastic sulfate reduction in the sulfate-methane transition of marine

sediments. *Geochim. Cosmochim. Acta* 254, 231–245. doi: 10.1016/j.gca.2019.03.016

Jing, H., Wang, R., Jiang, Q., Zhang, Y., and Peng, X. (2020). Anaerobic methane oxidation coupled to denitrification is an important potential methane sink in deep-sea cold seeps. *Sci. Total Environ.* 748, 142459. doi: 10.1016/j.scitotenv.2020.142459

Karl, D., Letelier, R., Tupas, L., Dore, J., Christian, J., and Hebel, D. (1997). The role of nitrogen fication in biogeochemical cycling in the subtropical north pacific ocean. *Nature* 388, 533–537. doi: 10.1007/b138051

Kim, B., and Zhang, Y. G. (2022). Methane hydrate dissociation across the oligocene–Miocene boundary. *Nat. Geosci.* 15:203-211. doi: 10.1038/s41561-022-00895-5

Komada, T., Burdige, D. J., Li, H. L., Magen, C., Chanton, J. P., and Cada, A. K. (2016). Organic matter cycling across the sulfate-methane transition zone of the Santa Barbara basin, California borderland. *Geochim. Cosmochim. Acta* 176, 259–278. doi: 10.1016/j.gca.2015.12.022

Kuypers, M. M. M., Marchant, H. K., and Kartal, B. (2018). The microbial nitrogen-cycling network. *Nat. Rev. Microbiol.* 16, 263–276. doi: 10.1038/nrmicro.2018.9

Laima, M. J. C. (1992). Extraction and seasonal variation of NH4+ pools in different types of coastal marine sediments. *Mar. Ecol. Prog. Ser.* 82, 75–84. doi: 10.3354/meps082075

LaRowe, D. E., and Van Cappellen, P. (2011). Degradation of natural organic matter: A thermodynamic analysis. *Geochim. Cosmochim. Acta* 75, 2030–2042. doi: 10.1016/j.gca.2011.01.020

Lehmann, M. F., Bernasconi, S. M., Barbieri, A., and McKenzie, J. A. (2002). Preservation of organic matter and alteration of its carbon and nitrogen isotope composition during simulated and *in situ* early sedimentary diagenesis. *Geochim. Cosmochim. Acta* 66, 3573–3584. doi: 10.1016/S0016-7037(02)00968-7

Lehmann, M. F., Sigman, D. M., McCorkle, D. C., Granger, J., Hoffmann, S., Cane, G., et al. (2007). The distribution of nitrate 15N/14N in marine sediments and the impact of benthic nitrogen loss on the isotopic composition of oceanic nitrate. *Geochim. Cosmochim. Acta* 71, 5384–5404. doi: 10.1016/j.gca.2007.07.025

Levin, L. A., Baco, A. R., Bowden, D. A., Colaco, A., Cordes, E. E., Cunha, M. R., et al. (2016). Hydrothermal vents and methane seeps: Rethinking the sphere of influence. *Front. Mar. Sci.* 3. doi: 10.3389/fmars.2016.00072

Libes, S. M., and Deuser, W. G. (1988). The isotope geochemistry of particulate nitrogen in the Peru upwelling area and the gulf of Maine. *Deep Sea Res. Part A Oceanogr. Res. Pap* 35, 517–533. doi: 10.1016/0198-0149(88)90129-X

Li, N., Feng, D., Chen, L., Wang, H., and Chen, D. (2016). Using sediment geochemistry to infer temporal variation of methane flux at a cold seep in the south China Sea. *Mar. Pet. Geol.* 77, 835–845. doi: 10.1016/j.marpetgeo.2016.07.026

Lim, Y. C., Lin, S., Yang, T. F., Chen, Y. G., and Liu, C. S. (2011). Variations of methane induced pyrite formation in the accretionary wedge sediments offshore southwestern Taiwan. *Mar. Pet. Geol.* 28, 1829–1837. doi: 10.1016/j.marpetgeo.2011.04.004

Lin, Z., Sun, X., Lu, Y., Strauss, H., Xu, L., Chen, T., et al. (2018a). Iron isotope constraints on diagenetic iron cycling in the taixinan seepage area, south China Sea. *J. Asian Earth Sci.* 168, 112–124. doi: 10.1016/j.jseaes.2018.01.007

Lin, Z., Sun, X., Peckmann, J., Lu, Y., Xu, L., Strauss, H., et al. (2016). How sulfate-driven anaerobic oxidation of methane affects the sulfur isotopic composition of pyrite: A SIMS study from the south China Sea. *Chem. Geol.* 440, 26–41. doi: 10.1016/j.chemgeo.2016.07.007

Lin, Z., Sun, X., Strauss, H., Eroglu, S., Böttcher, M. E., Lu, Y., et al. (2021). Molybdenum isotope composition of seep carbonates – constraints on sediment biogeochemistry in seepage environments. *Geochim. Cosmochim. Acta* 307, 56–71. doi: 10.1016/j.gca.2021.05.038

Lin, Z., Sun, X., Strauss, H., Lu, Y., Böttcher, M. E., Teichert, B. M. A., et al. (2018b). Multiple sulfur isotopic evidence for the origin of elemental sulfur in an iron-dominated gas hydrate-bearing sedimentary environment. *Mar. Geol.* 403, 271–284. doi: 10.1016/j.margeo.2018.06.010

Lin, Z., Sun, X., Strauss, H., Lu, Y., Gong, J., Xu, L., et al. (2017). Multiple sulfur isotope constraints on sulfate-driven anaerobic oxidation of methane: Evidence from authigenic pyrite in seepage areas of the south China Sea. *Geochim. Cosmochim. Acta* 211, 153–173. doi: 10.1016/j.gca.2017.05.015

Liu, J., Pellerin, A., Antler, G., Kasten, S., Findlay, A. J., Dohrmann, I., et al. (2020). Early diagenesis of iron and sulfur in bornholm basin sediments : the role of near-surface pyrite formation. *Geochim. Cosmochim. Acta* 34, 45–60. doi: 10.1016/j.gca.2020.06.003

Li, N., Yang, X., Peckmann, J., Zhou, Y., Wang, H., Chen, D., et al. (2021). Persistent oxygen depletion of bottom waters caused by methane seepage: Evidence from the south China Sea. *Ore Geol. Rev.* 129:103949. doi: 10.1016/j.oregeorev.2020.103949

Li, N., Yang, X., Peng, J., Zhou, Q., and Chen, D. (2018). Paleo-cold seep activity in the southern south China Sea: Evidence from the geochemical and geophysical records of sediments. *J. Asian Earth Sci.* 168, 106–111. doi: 10.1016/j.jseaes.2017.10.022

Macko, S. A., and Estep, M. L. F. (1984). Microbial alteration of stable nitrogen and carbon isotopic compositions of organic matter. *Org. Geochem.* 6, 787–790. doi: 10.1016/0146-6380(84)90100-1

Martens-Habbena, W., and Qin, W. (2022). Archaeal nitrification without oxygen(The single-cell organism can self-produce oxygen for ammonia oxidation). *Science* 375, 7–9.

McDonnell, S. L., Max, M. D., Cherkis, N. Z., and Czarnecki, M. F. (2000). Tectono-sedimentary controls on the likelihood of gas hydrate occurrence near Taiwan. *Mar. Pet. Geol.* 17, 929–936. doi: 10.1016/S0264-8172(00)00023-4

Meister, P., Liu, B., Khalili, A., Böttcher, M. E., and Jørgensen, B. B. (2019). Factors controlling the carbon isotope composition of dissolved inorganic carbon and methane in marine porewater: An evaluation by reaction-transport modelling. *J. Mar. Syst.* 200, 103227. doi: 10.1016/j.jmarsys.2019.103227

Miao, X., Feng, X., Li, J., and Lin, L. (2021). Tracing the paleo-methane seepage activity over the past 20,000 years in the sediments of qiongdongnan basin, northwestern south China Sea. *Chem. Geol.* 559, 119956. doi: 10.1016/j.chemgeo.2020.119956

Middelburg, J. J. (1989). A simple rate model for organic matter decomposition in marine sediments. *Geochim. Cosmochim. Acta* 53, 1577–1581. doi: 10.1016/0016-7037(89)90239-1

Nakatsuka, T., Handa, N., Harada, N., Sugimoto, T., and Imaizumi, S. (1997). Origin and decomposition of sinking particulate organic matter in the deep water column inferred from the vertical distributions of its δ15N, δ13 and δ14. *Deep Sea Res. Part I Oceanogr. Res. Pap.* 44, 1957–1979. doi: 10.1016/s0967-0637(97)00051-4

Panieri, G., Lepland, A., Whitehouse, M. J., Wirth, R., Raanes, M. P., James, R. H., et al. (2017). Diagenetic mg-calcite overgrowths on foraminiferal tests in the vicinity of methane seeps. *Earth Planet. Sci. Lett.* 458, 203–212. doi: 10.1016/j.epsl.2016.10.024

Peckmann, J., Birgel, D., and Kiel, S. (2009). Molecular fossils reveal fluid composition and flow intensity at a Cretaceous seep. *Geology* 37, 847–850. doi: 10.1130/G25658A.1

Peckmann, J., and Thiel, V. (2004). Carbon cycling at ancient methane-seeps. *Chem. Geol.* 205, 443–467. doi: 10.1016/j.chemgeo.2003.12.025

Peckmann, J., Thiel, V., Reitner, J., Taviani, M., Aharon, P., and Michaelis, W. (2004). A microbial mat of a large sulfur bacterium preserved in a miocene methane-seep limestone. *Geomicrobiol. J.* 21, 247–255. doi: 10.1080/01490450490438757

Peckmann, J., Walliser, O. H., Riegel, W., and Reitner, J. (1999). Signatures of hydrocarbon venting in a middle Devonian carbonate mound (Hollard mound) at the hamar laghdad (Antiatlas, Morocco). *Facies* 40, 281–296. doi: 10.1007/BF02537477

Quan, T. M., Adigwe, E. N., Riedinger, N., and Puckette, J. (2013a). Evaluating nitrogen isotopes as proxies for depositional environmental conditions in shales: Comparing caney and woodford shales in the arkoma basin, Oklahoma. *Chem. Geol.* 360–361, 231–240. doi: 10.1016/j.chemgeo.2013.10.017

Quan, T. M., Wright, J. D., and Falkowski, P. G. (2013b). Co-Variation of nitrogen isotopes and redox states through glacial-interglacial cycles in the black Sea. *Geochim. Cosmochim. Acta* 112, 305–320. doi: 10.1016/j.gca.2013.02.029

Reeburgh, W. S. (2007). *Oceanic methane biogeochemistry* (Irvine, California: Department of Earth System Science, University of California). doi: 10.1021/cr050362v

Regnier, P., Dale, A. W., Arndt, S., LaRowe, D. E., Mogollón, J., and Van Cappellen, P. (2011). Quantitative analysis of anaerobic oxidation of methane (AOM) in marine sediments: A modeling perspective. *Earth-Science Rev.* 106, 105–130. doi: 10.1016/j.earscirev.2011.01.002

Robinson, R. S., Kienast, M., Luiza Albuquerque, A., Altabet, M., Contreras, S., De Pol Holz, R., et al. (2012). A review of nitrogen isotopic alteration in marine sediments. *Paleoceanography* 27:4203. doi: 10.1029/2012PA002321

Ruppel, C. D. (2017). The interaction of climate change and methane hydrates. *Rev. Geophys.* 55, 126–168. doi: 10.1002/2016RG000534

Schrum, H. N., Spivack, A. J., Kastner, M., and D'Hondt, S. (2015). Sulfate-reducing ammonium oxidation: A thermodynamically feasible metabolic pathway in subseafloor sediment. *Geology* 37, 939–942. doi: 10.1130/G30238A.1

Suess, E. (2010). Handbook of hydrocarbon and lipid microbiology. *Handb. Hydrocarb. Lipid Microbiol.* Springer-Verlag Berlin Heidelberg doi: 10.1007/978-3-540-77587-4

Suess, E. (2014). Marine cold seeps and their manifestations: geological control, biogeochemical criteria and environmental conditions. *Int. J. Earth Sci.* 103, 1889–1916. doi: 10.1007/s00531-014-1010-0

Suess, E. (2020). Hydrocarbons, oils and lipids: Diversity, origin, chemistry and fate. *Hydrocarb. Oils Lipids Divers. Orig. Chem. Fate.* Springer International Publishing AG doi: 10.1007/978-3-319-90569-3

Tesdal, J. E., Galbraith, E. D., and Kienast, M. (2013). Nitrogen isotopes in bulk marine sediment: Linking seafloor observations with subseafloor records. *Biogeosciences* 10, 101–118. doi: 10.5194/bg-10-101-2013

Thullner, M., Regnier, P., and Van Cappellen, P. (2007). Modeling microbially induced carbon degradation in redox-stratified subsurface environments: Concepts and open questions. *Geomicrobiol. J.* 24, 139–155. doi: 10.1080/01490450701459275

Tong, H., Feng, D., Cheng, H., Yang, S., Wang, H., Min, A. G., et al. (2013). Authigenic carbonates from seeps on the northern continental slope of the south China Sea: New insights into fluid sources and geochronology. *Mar. Pet. Geol.* 43, 260–271. doi: 10.1016/j.marpetgeo.2013.01.011

van Dongen, B. E., Roberts, A. P., Schouten, S., Jiang, W. T., Florindo, F., and Pancost, R. D. (2007). Formation of iron sulfide nodules during anaerobic oxidation of methane. *Geochim. Cosmochim. Acta* 71, 5155–5167. doi: 10.1016/j.gca.2007.08.019

Wang, X., Li, N., Feng, D., Hu, Y., Bayon, G., Liang, Q., et al. (2018b). Using chemical compositions of sediments to constrain methane seepage dynamics: A case study from haima cold seeps of the south China Sea. *J. Asian Earth Sci.* 168, 137–144. doi: 10.1016/j.jseaes.2018.11.011

Wang, T., Ravelo, A. C., Ren, H., Dang, H., Jin, H., Liu, J., et al. (2018a). Nitrogen isotope variations in the northern south China Sea since marine isotopic stage 3: Reconstructed from foraminifera-bound and bulk sedimentary nitrogen. *Paleoceanogr. Paleoclimatology* 33, 594–605. doi: 10.1029/2018PA003344

Wehrmann, L. M., Risgaard-Petersen, N., Schrum, H. N., Walsh, E. A., Huh, Y., Ikehara, M., et al. (2011). Coupled organic and inorganic carbon cycling in the deep subseafloor sediment of the northeastern Bering Sea slope (IODP exp. 323). *Chem. Geol.* 284, 251–261. doi: 10.1016/j.chemgeo.2011.03.002

Wu, S., Wang, X., Wong, H. K., and Zhang, G. (2007). Low-amplitude BSRs and gas hydrate concentration on the northern margin of the south China Sea. *Mar. Geophys. Res.* 28, 127–138. doi: 10.1007/s11001-007-9020-y

Wu, D., Wu, N., Fu, S., Lian, J., and Hongxiang, G. (2010). Geochemicalcharacteristic of shallow sediments in the gas hydrate distribution area of dongsha, the northern south China Sea. *Mar. Geol. Quat. Geol.* 30, 41–51. doi: 10.3788/HPLPB20102209.2186

Xie, R., Wu, D., Liu, J., Sun, T., Liu, L., and Wu, N. (2019). Evolution of gas hydrates inventory and anaerobic oxidation of methane (AOM) after 40ka in the taixinan basin, south China Sea. *Deep Sea Res. Part I Oceanogr. Res. Pap*, 152:103084. doi: 10.1016/j.dsr.2019.103084

Xiong, P., Lu, H., Xie, X., Zhang, G., Fu, S., Jiang, L., et al. (2020). Geochemical responses and implications for gas hydrate accumulation: Case study from site SHC in shenhu area within northern south China Sea. *Mar. Pet. Geol.* 111, 650–661. doi: 10.1016/j.marpetgeo.2019.06.032

Xu, F., Hu, B., Zhao, J., Liu, X., Xu, K., Xiong, Z., et al. (2021). Provenance and weathering of sediments in the deep basin of the northern south China Sea during the last 38 kyr. *Mar. Geol.* 440, 106602. doi: 10.1016/j.margeo.2021.106602

Yang, T., Jiang, S. Y., Ge, L., Yang, J. H., Wu, N. Y., Zhang, G. X., et al. (2010). Geochemical characteristics of pore water in shallow sediments from shenhu area of south China Sea and their significance for gas hydrate occurrence. *Chin. Sci. Bull.* 55, 752–760. doi: 10.1007/s11434-009-0312-2

Yang, X., Sun, X., Li, D., Lin, Z., Lu, Y., Liang, Y., et al. (2020). Elemental and isotopic response of different carbon components to anaerobic oxidation of methane: A case study of marine sediments in the shenhu region, northern south China Sea. *J. Asian Earth Sci.* 206, 104577. doi: 10.1016/j.jseaes.2020.104577

Zhang, X., Gong, J., Sun, Z., Liao, J., Zhai, B., Wang, L., et al. (2021). Pore-water geochemistry in methane-seep sediments of the makran accretionary wedge off Pakistan: Possible link to subsurface methane hydrate. *Acta Oceanol. Sin.* 40, 23–32. doi: 10.1007/s13131-021-1899-7

Zhang, G., Liang, J., Lu, J., Yang, S., Zhang, M., Holland, M., et al. (2015). Geological features, controlling factors and potential prospects of the gas hydrate occurrence in the east part of the pearl river mouth basin, south China Sea. *Mar. Pet. Geol.* 67, 356–367. doi: 10.1016/j.marpetgeo.2015.05.021

Zhang, M., Lu, H., Guan, H., Liu, L., Wu, D., and Wu, N. (2018). Methane seepage intensities traced by sulfur isotopes of pyrite and gypsum in sediment from the shenhu area, south China Sea. *Acta Oceanol. Sin.* 37, 20–27. doi: 10.1007/s13131-018-1241-1

Zhang, Y., Luo, M., Hu, Y., Wang, H., and Chen, D. (2019). An areal assessment of subseafloor carbon cycling in cold seeps and hydrate-bearing areas in the northern south China Sea. *Geofluids* 2019:2573937. doi: 10.1155/2019/2573937

Zhang, T., Xiao, X., Chen, S., Zhao, J., Chen, Z., Feng, J., et al. (2020). Active anaerobic archaeal methanotrophs in recently emerged cold seeps of northern south China Sea. *Front. Microbiol.* 11:612135. doi: 10.3389/fmicb.2020.612135

Zhuang, C., Chen, F., Cheng, S. H., Lu, H. F., Wu, C., Cao, J., et al. (2016). Light carbon isotope events of foraminifera attributed to methane release from gas hydrates on the continental slope, northeastern south China Sea. *Sci. China Earth Sci.* 59, 1981–1995. doi: 10.1007/s11430-016-5323-7